Colloid Polym Sci 280:389–397 (2002)

ORIGINAL CONTRIBUTION

Joachim Götz
Ralf Zimehl

Shear and NMR experiments of materials with flow behaviour depending on the deformation history

Received: 19 July 2001
Accepted: 25 October 2001

J. Götz (✉)
Lehrstuhl für Brauereianlagen und
Lebensmittel-Verpackungstechnik
TU München, Weihenstephaner Steig 22
85350 Freising-Weihenstephan, Germany
e-mail: joachim.goetz@bl.tum.de

R. Zimehl
Institut für Anorganische Chemie,
Christian-Albrechts-Universität Kiel
Olshausenstrasse 40, 24098 Kiel, Germany

Abstract Oxide ceramic masses react to simple shearing with hardening (peptisation: increase in the shear stress with the shear deformation). In the present study the correlation between the increase in the shear stress and the porosity, agglomeration processes and the type of flow are analysed. For this purpose oxide ceramic masses are tested in a shear device especially developed for pastes and analysed by rheometric experiments, NMR methods and particle size analysis. The results support the hypothesis that structural changes (hardening, increase in the mean porosity) of the material during the peptisation mainly depend on the magnitude and not on the kind of the energy input and thus of the type of flow. The fraction of bound (more generally, the immobilised) water increases with the shear displacement. Also crushing of primary particles could be observed. Both the crushing of solid particles causing an increased solid surface and the formation of a three-dimensional gel structure are microscopic effects capable of resulting in the binding or retaining water. On a macroscopic scale these phenomena cause hardening. Magnetic resonance imaging visualises flow-induced agglomerates, which form owing to the shear flow and increase the porosity averaged over the whole sample. After the shear experiment rolls of paste can be seen which indicate that the general assumption of a plane shear flow in the shear device is not warrantable.

Keywords Hardening · Oxide ceramics · Shear flow · NMR · Particle size analysis

Introduction

The rheological behaviour of high solid dispersions and slurries is extremely complex [1–16]. Microscopically, the slurry can be regarded as a colloid, but a very simple question soon arises for these kinds of colloidal systems: Is this colloid formed from solid particles or flocs of solid particles dispersed in a liquid (discontinuous system), or is it rather a bicontinuous system, in which strings of particles and very thin liquid films interpenetrate? Eventually there also are gaseous inclusions in the jelly matrix of these systems and the macroscopic properties of the slurry are influenced by the characteristics of each phase as well as by their interactions. To characterise the flow behaviour of the slurries, shear experiments were run on an shear device especially designed in order to investigate the normal stress-dependent flow behaviour of pastes and highly concentrated suspensions [17–19]. With this equipment it was found that for sufficient shear deformation and below a critical degree of moisture, oxide ceramic pastes undergo shear-dependent hardening (rheopexy), i.e., an increase in the shear stress with the shear deformation at constant normal stress. In the rheology of slurries and pastes, this phenomenon is called peptisation.

Besides the hardening, a noticeable increase in the porosity can be found. In this article the correlation of peptisation, agglomeration and the kind of energy input into the material, i.e., the flow type, is studied. After the shear experiment, which was used for both rheological characterisation and material preparation, samples were taken and examined with NMR techniques and particle size analysis. With NMR it is possible [18] both to locate patterns of moisture which can be interpreted as agglomerates within the sheared paste (magnetic resonance imaging, MRI) and to determine both the fraction of a phase of water (e.g., free or immobile water) of the local total moisture and the type of bond of the ^{1}H protons in this phase (NMR spectroscopy).

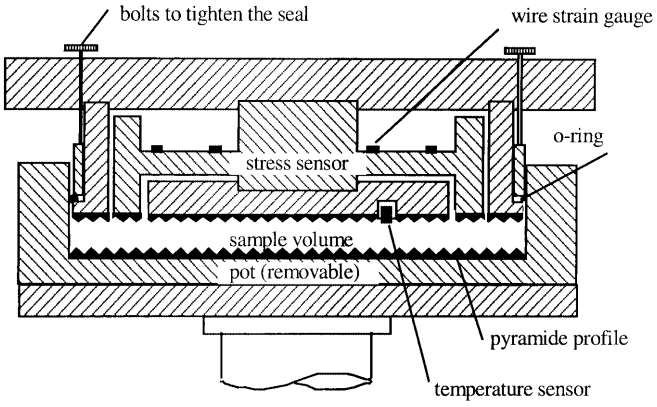

Fig. 1 Schematic of the shear cell

Experimental

Materials

The experiments were performed with Pural SB (Condea, Brunsbüttel, Germany). The solid material is used in large amounts for the preparation of catalysts and catalyst carriers. Pural SB was chosen because there is already a considerable amount of data available concerning the extrusion, the crack and the flow behaviour in shear flows. It was supplied as a spray-dried aluminium oxide/hydroxide (boehmite alumina) with a specific surface of 285 m^2g^{-1} (laser-diffraction-based Helos particle analyser, Sympatec, Clausthal-Zellerfeld). The porous agglomerates have a d_{50} of 46 μm (mercury porosimetry). Aluminium oxide/hydroxide slurries were prepared by mixing weighed amounts of Pural SB with distilled water by means of a common household stirrer (Philips HR1453). As both components were weighed individually and then subsequently mixed, the moisture content in the slurry is most conveniently defined as

$$F = \frac{m_{\text{liquid}}}{m_{\text{solid}} + m_{\text{liquid}}} \quad , \tag{1}$$

where m_{liquid} is the mass of water and m_{solid} is the mass of dried aluminium oxide/hydroxide.

Measurement of the flow properties

The shear device developed and designed by Felder [17] (Fig. 1) consists of two parallel plates that can be concentrically twisted against each other. The lower plate of the device is formed like a pot (inner diameter: 160 mm, height: 38 mm). The lid and the bottom of the pot are profiled with pyramids (height: 2 mm, angle: 90) in order to avoid wall slip and enforce an inner shearing of the test material. The slit between the rotating pot and the immovable lid can be sealed by an adjustable O-ring that ensures a hermetically sealed volume. This is necessary, because otherwise fluid constituents of the specimen would be pressed out of the shear cell during the shear experiment. This is a great problem when applying conventional rheometric methods, for example, plate–plate, plate–cone or capillary rheometry, because even the mean moisture generally changes during the shear experiment owing to a possible loss of fluid. As the flow behaviour of pastes usually depends on the moisture, the flow of fluid out of the measuring volume and thus conventional rheometric techniques are not acceptable.

The upper plate is divided into three concentric parts. The normal force and the torque on the ring in the middle (inner diameter: 108 mm, outer diameter: 131 mm) can be measured and converted into normal stress and shear stress. With this construction of the measuring device, the forces needed to seal the lid and the pot do not have any effect on the measurement of normal and shear stress.

Three types of experiments were performed. In case a, simple shearing was maintained with a constant shearing direction, whereas in case b shearing with changing direction (“oscillating”) was performed. The shear displacement in case a was 60 m. In case b, the sum of the magnitude of the shear displacements was also 60 m. The direction of the rotating velocity of the measuring ring changed after 25 s with a break of 1 s. For case c, the paste was kneaded in a torque rheometer (Plasti-Corder P1151) before the measurements with simple shearing and constant shearing directions were performed.

Calculation of the energy input

The average distance between the ring and the bottom of the pot, which is not fixed like the normal stress during an experiment (Fig. 1), is about 10 mm and the rotation velocity of the ring was set to 25 mms^{-1}; therefore, the quotient of the ring velocity and the average slit width, i.e., the mean shear rate, was about 2.5 s^{-1} for all the experiments. Thus, the energy input into the material at simple shearing can be calculated by

$$E = \int \tau(t) v(t) A \mathrm{d}t \quad \text{or} \quad E = \int \tau(s) A \mathrm{d}s \ . \tag{2}$$

In Eq. (2) $\tau(t)$ or $\tau(s)$ is the shear stress, $v(t)$ is the velocity of the rotating measuring ring and A is the area of the measuring ring. The energy input into the probe when kneaded can be derived from the torque, M, and the angular velocity, ω, of the kneading device:

$$E = \int M(t)\ \omega(t)\ \mathrm{d}t \ . \tag{3}$$

From Eqs. (2) and (3) the volume-specific energy, w, related to the volume, V, of the specimen can be calculated by

$$w = \frac{E}{V} \ . \tag{4}$$

NMR measurements of the slurries

NMR [20–23] stems from the fact that the nuclei of specific isotopes (e.g., of the hydrogen isotope ^{1}H) possess a magnetic moment (spin) and precess under a specific angle with respect to an external magnetic field:

$$\mathbf{B}_0 = B_0(0, 0, 1) \ . \tag{5}$$

In the case of spin 1/2 nuclei their components along the field axis ($\mathbf{B}_0$) are either parallel or antiparallel to $\mathbf{B}_0$. As the parallel orientation is (for ^{1}H) energetically preferable, this orientation is assumed by a larger number of nuclear spins. Irridiation at the Larmor frequency, ω, of which the energy difference $\Delta E = h\omega$ is equivalent to the difference between the two energy levels, changes the orientation of the surplus spins in the lower energy level. The absorbed energy can be measured. The Larmor frequency can be expressed as

$$\omega = \gamma \mathbf{B}_0, \tag{6}$$

where γ is the gyromagnetic ratio, which is specific for the nucleus used. The resonance frequency of ^{1}H is 42.55 MHz for $\mathbf{B}_0 = 1$ T. The fundamentals of NMR will not be considered further here, but only the results provided by the technique.

After the shear experiments, samples were taken out of the shear device and analysed with 1D NMR spectra [24]. The NMR experiments described here were performed in a SWB200 magnet (Bruker Analytik, Rheinstetten, Germany). The static magnetic field, $\mathbf{B}_0$, is 4.7 T, which corresponds to a proton frequency of 200.13 MHz. The radial and axial extensions of the measuring volume with a homogeneous magnetic field are 40 mm.

The NMR spectrum is the frequency distribution, $g(\omega)$, of nuclei with a resonance frequency ω. Fitting the NMR spectrum of a material with a sum of Gaussian functions provides the fraction of the water phase of the total degree of moisture as the integral of the respective Gaussian function and the bonding type of the water phase that can be characterised by the half-width of the corresponding Gaussian function [24, 25]. This NMR technique yields not only the nucleus concentration (^{1}H), and thus the moisture, but also information concerning the bonding type of the fluid to the solid and the distribution of the total moisture between the phases (MRI). As such, it is possible to distinguish between free and immobilised (''bound'') water (e.g., crystallisation water, pore water) and free water [25, 26]. Several measuring strategies have been developed for the effective determination of the spatial distribution of the hydrogen (generally of the nuclei used) density. A detailed description of MRI sequences with regard to their capabilities and limitations is given in Refs. [23, 27]. In every MRI experiment the sample was divided into a grid (matrix) of three-dimensional voxels. The size of each voxel is given by the chosen so-called field of flow, which means the dimensions of the measuring volume in the magnet and the matrix size (number of voxels according to the relevant spatial dimensions). The resolution of the images is 30 μm with a matrix size of 256×256. The NMR test glass has an outer diameter of 5 mm and an inner diameter of 4 mm. The (global or local) fluid volume concentration (fluid fraction), c_F, that can be determined with MRI is

$$c_F = \frac{V_{liquid}}{V}\ , \tag{7}$$

where V is the volume of a voxel and V_{liquid} is the fluid volume in the complete sample (global) or in the same voxel (local), respectively.

Results

Pural pastes with different degrees of moisture were used for the shear experiments. The rotating velocity of the ring in all cases was 25 mms^{-1}. Three different types of flows – and thus of loadings – were chosen. In case a, simple shearing was maintained with a constant shearing direction, whereas in case b shearing with changing direction (oscillating loading) was performed. The shear displacement in case a was 60 m. In case b, the sum of the magnitude of the shear displacements was also 60 m. The direction of the rotating velocity of the measuring ring changed after 25 s with a break of 1 s. For case c the paste was kneaded in a torque rheometer (Plasti-Corder P1151) before the measurements with simple shearing and constant shearing direction were performed. A typical temporal development of the torque in the kneader is shown in Fig. 2.

After an initial phase of thixotropy the material hardens continuously. The finally kneaded probe was then examined in the experimental shear device, at simple shearing and constant normal stress. The results of the measurements are presented in Figs. 3 and 4. For the slurries with an average degree of moisture $F = 66$ % (Fig. 3a) and $F = 72\%$ (Fig. 3b) the curves of the shear stress, $\tau(s)$, versus shear displacement, s, are independent of the type of energy input. The results for simple shearing (case a) and oscillating shear (case b) for the normal stress, $\sigma = 60$ kPa, and the constant degree of moisture are similar in magnitude.

From Fig. 4 it can be seen that the results for simple shearing (case a) and oscillating shear (case b) at different normal stress and $F = 70\%$ are also in good agreement, which means that the change of the shear direction does not influence the temporal evolution of the shear stress.

In Fig. 5 the shear stress τ – as a function of the shear displacement $\tau = f(s)$ – is compared for experiments of case a (simple shearing of the paste) and for experiments of case c, i.e., the paste is kneaded in a torque rheometer before the shearing. There are no significant differences in the temporal development. The $\tau(s)$ curves of the experiments for case c are displaced, compared to case a, by that displacement at which the same energy in the simple shearing (case a) was input into the material as by the kneading process.

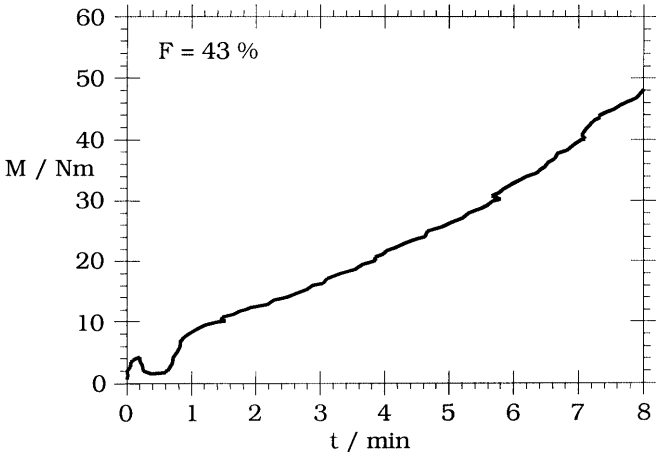

Fig. 2 Torque, M, in a kneader for a Pural paste, $F = 43\%$

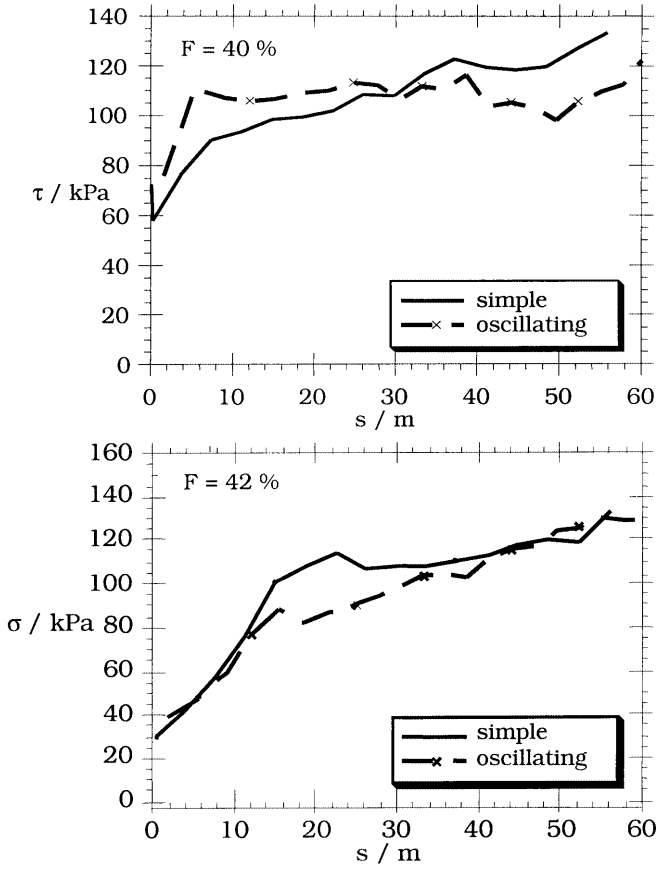

Fig. 3 Simple and oscillating shear experiment at $\sigma = 60$ kPa. Parameter: F

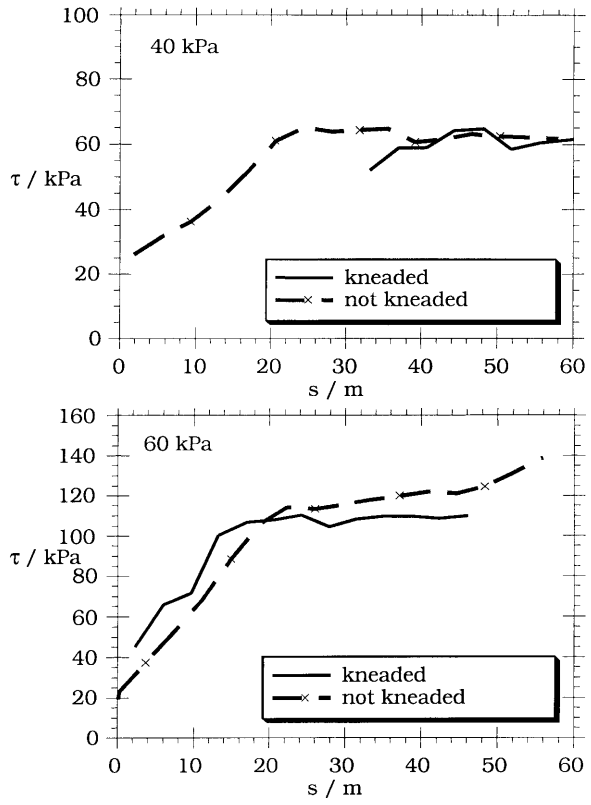

Fig. 5 Simple shearing of kneaded and unkneaded samples. The shear curves of the kneaded samples are displaced for that shear deformation, when the same work in the simple shear flow is done as during the kneading. $F = 41\%$. Parameter: σ

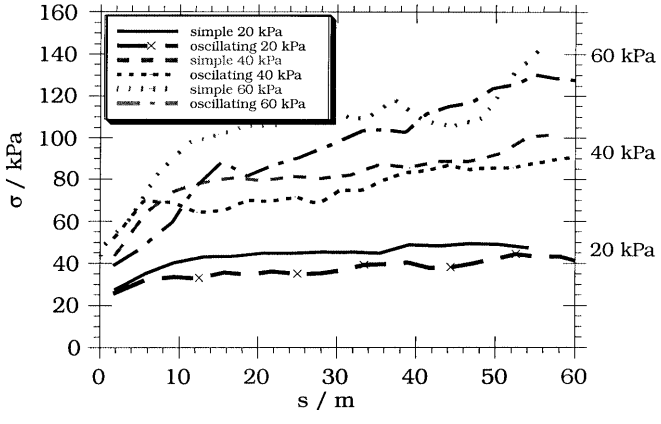

Fig. 4 Simple and oscillating shear experiment, $F = 41\%$. Parameter: σ

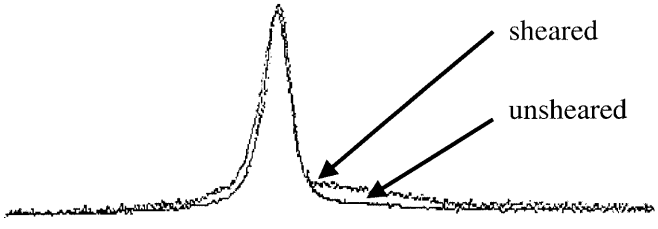

Fig. 6 NMR spectrum of Pural, $F = 33\%$. *Lower spectrum*: Unsheared. *Upper spectrum*: Sheared in a simple shear flow with $\sigma = 100$ kPa

After the shear experiments, the samples were taken out of the shear device and analysed with NMR and MRI. With NMR it is possible to distinguish between free and immobilised water (e.g., crystallisation water, pore water) and free water. A typical result of these experiments can be seen in Fig. 6 for a Pural slurry with an average degree of moisture $F = 50\%$. In order to derive the ratio of the immobilised fraction of water to the free water the spectra were fitted with a sum of two Gaussian functions. The half-width of the single Gaussian functions is the measure to distinguish water with regard to its mobility and hence its bonding type to the solid. The smaller the half-width, the bigger the mobility and the weaker the bonding type of the water to the solid. According to the theory described in Abragam [24] and the more detailed theory of, for example, Zimmer-

man and Brittin [26] and Hills et al. [25] the phase with the greater half-width stands for the immobile water phase and the smaller half-width corresponds to free water. An exception is the water of crystallisation, the spectrum of which does not a have Gaussian form [24].

A comparison of the NMR spectra ($F = 50\%$) of a sheared probe ($\sigma = 100$ kPa, $s = 60$ m) with an original unsheared probe shows that the integral of the wide distribution (i.e., the immobilised water) increases with an increase oin the shear deformation, i.e., with the progression of the hardening. This means that the fraction of immobilised water increases with increasing energy input. From Fig. 6 it can be seen that the immobilised water in Pural pastes is not water of crystallisation. The water molecules for water of crystallisation have well-defined places in the lattice, whereas the protons of water immobilised in a different way still have a certain mobility on the surface of the solid particles.

Several explanations for an increase in the fraction of immobilised water are imaginable:

1. Crushing of agglomerates of the solid primary particles and, hence, increasing of the specific surface (related to the solid mass).
2. Formation of a three-dimensional structure that is able to immobilise water.
3. Drainage of water in the interior of the solid particles, possibly in combination with adsorption at the particle surface.

As already mentioned Pural is a spray-dried aluminium oxide/hydroxide with a comparably high specific surface of 285 m^2g^{-1}. Owing to this very high specific surface Pural is capable of binding water in considerable amounts. As a result of the energy input an increased ratio of the solid surface might become available for immobilising water as a result of a mechanical effect.

To elucidate the different hypotheses the mean particle size, d_{50}, was determined as a function of the shear displacement, s, in the simple shearing experiment (case a). After the shear experiments, samples of the pastes were dispersed in water with the help of an ultrasonic bath (5 min) in order to destroy agglomerates formed during the shear experiment. The dispersion thus prepared was tested in a laser-diffraction-based particle analyser (Helos, Sympatec, Clausthal-Zellerfeld). The result of the experiment is shown in Fig. 7. A noticeable reduction in d_{50} for the primary particles can be observed (about a factor 4 compared to the original size) which indeed suggests explanation 1 to be operative. On the other hand, the surfaces of the boehmite particles in the Pural could be hydrolysed to aluminium hydroxide gel [28]. The optimal dispersing of the paste in the shear tester or kneader – achieved by sufficient energy input by shearing or kneading – might be the prerequisite or the acceleration for the gelation process, i.e., the peptisation. Thus, the crushing of agglomerates

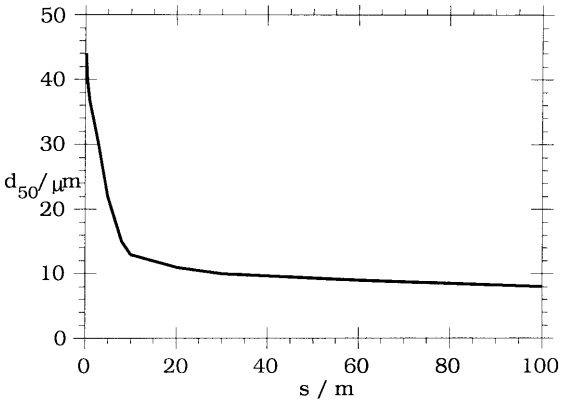

Fig. 7 d_{50} of a Pural paste as function of the shear deformation, s. The paste was dispersed in an ultrasonic bath (5 min). $F = 33\%$, $\sigma = 100$ kPa

of primary particles, cf. explanation 1, could additionally intensify the peptisation. Explanation 3, the drainage of water into the interior of the alumina particles, might additionally happen in the case of Pural.

Lightweight concrete is a material system where the drainage of fluid into the solid particles plays an important role. Usually lightweight concrete tends to choke a pipe when being pumped [29]. The reason for this phenomenon is that water plus cement partly drains into the porous particles (e.g., burned clay pellets) used as substitutes for gravel. Commercially available burned clay pellets have a porosity up to 50 vol% and, therefore, have a big capacity to retain fluid. The drainage of fluid into solid particles causes, like the phenomena described in explanations 1and 2, time-dependent flow behaviour.

The fraction of immobilised water, ϕ_{im}, derived by fitting the NMR spectra of Pural pastes with the sum of two Gaussian functions is plotted as a function of the shear displacement, s, the energy input, E, and the shear stress, τ, in Fig. 8a, b and c, respectively. Apparently, more and more water is bound to or immobilised by the solid matrix and ϕ_{im} increases with increasing values of s and E. For $\tau > 90$ kPa, ϕ_{im} increases continuously with τ. For large shear deformations, τ (Figs. 3, 4, 5) as well as ϕ_{im} (Fig. 8a) seem to approach a limit, probably given by the solid matter available. From a macroscopic point of view this process can be described as hardening.

Besides this hardening process, in many shear experiments a noticeable increase of the distance between the lid (measuring ring) and the base of the pot of the shear cell was observed. Thus, with the knowledge of the volumes of the solid and fluid constituents the porosity, ε, of the total system is derived from the distance between the two shearing plates (Fig. 9).

In order to characterise shear-induced structural changes, probes were taken before and after the experiment for analysis with MRI (Fig. 10). The resolution of

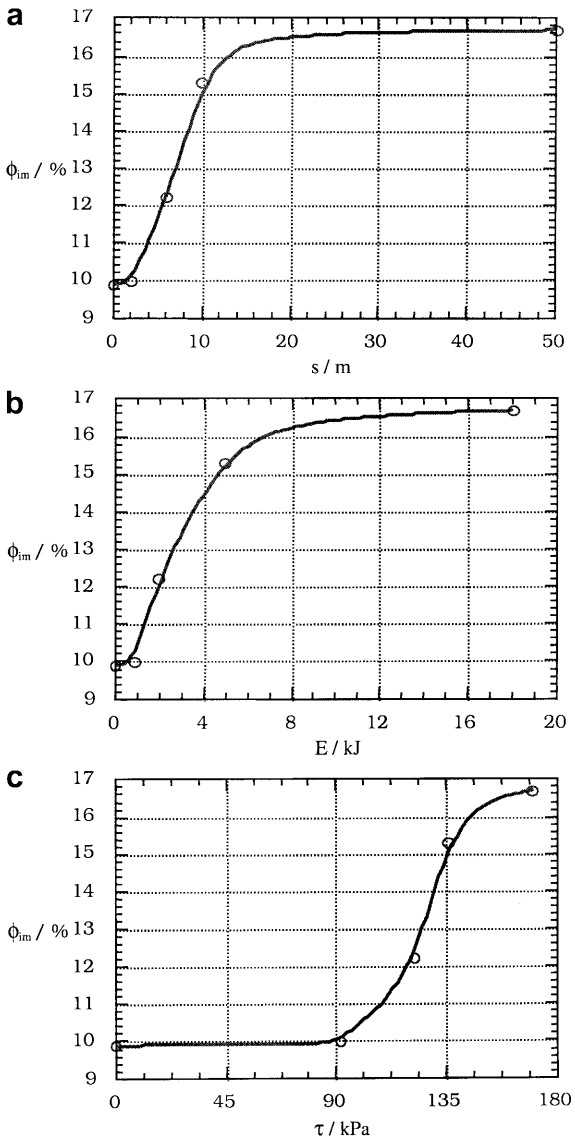

Fig. 8a–c Simple shear flow of a Pural paste: $\sigma = 100$ kPa, $F = 33\%$. Immobilised phase, ϕ_{im}, as function of **a** the shear displacement, s, **b** the energy input, E, and **c** the corresponding yield stress, τ

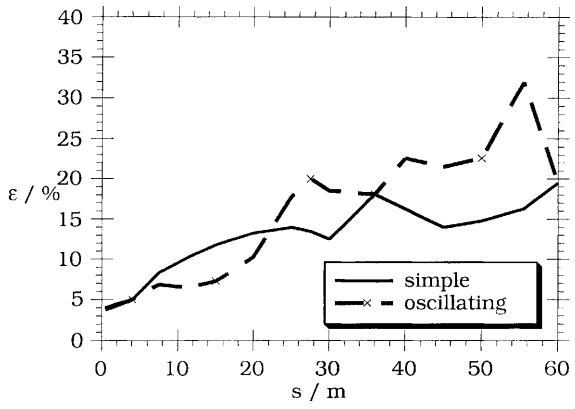

Fig. 9 Porosity, ε, of a Pural paste as a function of the shear deformation, s. $F = 33\%$. Loadings: Simple shearing, shearing with oscillating shear direction

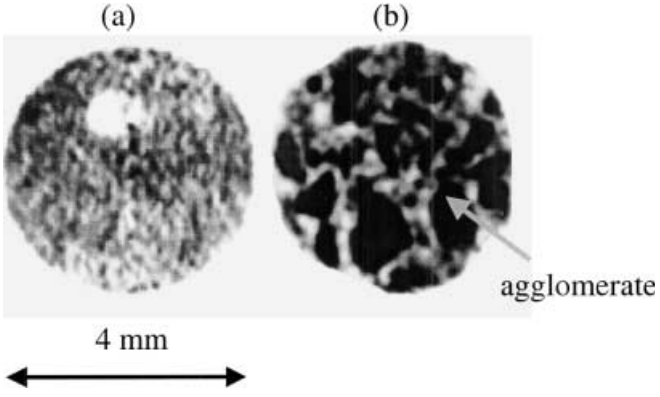

Fig. 10 Local fluid volume concentration, c_F, of **a** an unsheared and **b** a sheared Pural paste ($F = 33\%$, $s = 60$ m, $\sigma = 100$ kPa). The inner diameter of the sample tube is 4 mm. The local intensity of the magnetic resonance imaging images is proportional to the local volume concentration of ^{1}H nuclei, i.e., is proportional to c_F. The *bright areas* indicate no fluid and the darker the intensity, the higher the fluid concentration

the images is 40 μm with a matrix size of 128 × 128. The local intensity of the MRI images shown here is proportional to the local volume concentration of ^{1}H nuclei, i.e., proportional to the local fluid concentration, c_F. Bright areas indicate no fluid and the darker the intensity, the higher the fluid concentration. A Pural paste ($F = 50\%$) that has not been sheared is shown in Fig. 10a. c_F is – at a spatial resolution of 40 μm – almost homogeneous in the material. After the shear experiment ($s = 60$ m, $\sigma = 100$ kPa) the paste has a completely different structure (Fig. 10b). A moisture pattern can clearly be seen. That means that not only the fraction of immobilised water increases during the peptisation (Figs. 6, 8), but also that the water concentrates in structures – most likely agglomerates – of approximately 1 ml in size (Fig. 10b). Orientation processes of the aggregates in shear flow cannot be observed in the samples studied.

The composition of the crumbly structure (Fig. 10b) also seems to be responsible for the increase of the mean porosity during the peptisation (Fig. 9). There is another effect that obviously contributes to the increase of the mean porosity during the shear experiment. In some experiments the paste rolls in single isolated cylinders positioned like a star in the shear cell (Fig. 11) [18]. The formation of this macroscopic structure causes a further increase of the mean porosity. The introduction of air into the sample, the formation of hollow spaces or an eventual tearing apart of the sample (as, for example, observed in shear experiments on fat or ointments [3])

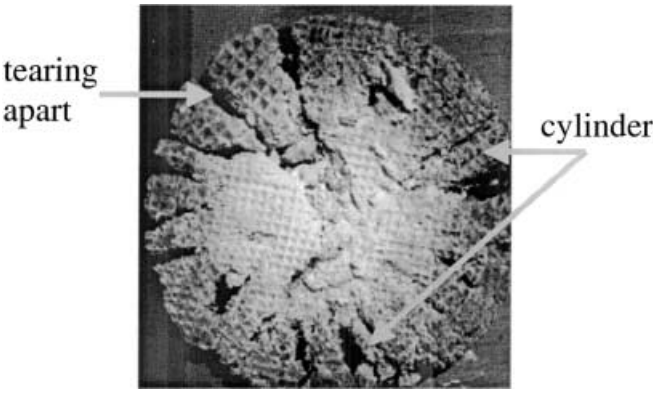

Fig. 11 Photograph of a sheared Pural paste: $s = 60$ m, $\sigma = 100$ kPa, $F = 33\%$

causes, furthermore, an increase in porosity (i.e., the increase in distance between the plates). As a further consequence these effects reveal that the paste has not flowed in a simple shear flow, as assumed. The flow pattern is more complex than a simple shear flow.

Discussion

We have presented the results of experiments performed on Pural pastes under different conditions. The loading, i.e., the type of flow, and the manner of preparation was varied from simple shearing and mixing by hand or shearing with changing directions and mixing by hand to simple shearing and kneading of the probes before the shear experiments. The good agreement of $\tau(s)$ of the three experiment types suggests that the constitutive law of a Bingham fluid [30] can be applied for general types of flow, not only for simple shear flow. This means that the materials could be modelled as Bingham fluids, i.e.,

$$\tau = \tau_0 + \eta_B \kappa \ . \tag{8}$$

In this equation τ_0 is the yield stress, η_B is the Bingham viscosity and κ is the shear rate. If the viscous stress can be neglected in comparison with the yield stress, the evolution of the shear stress, $\tau(s)$, as a function of the displacement, s, shows the dependency of τ_0 of the shear deformation, s, the normal stress, σ, and the moisture, F. τ_0, however, can no longer be considered as a material constant. It is a function of the local history of deformation, σ and the local degree of moisture, c_F. For rigid/plastic materials [31] the work-hardening hypothesis was suggested earlier by Schmidt [32].

Viscoplastic materials play also an important role in food technology. Schluentz et al. [33] and Campo et al. [34] investigated the rheology and the microstructure of several food products with strain-history-dependent flow behaviour developed with controlled deformation. The results were compared with dynamic rheological properties to evaluate the influence of strain deformation on the formation of microstructure. The results were significantly different between shear-strained and extensionally strained samples.

Pural pastes, however, show comparable flow and hardening behaviour in the three flow types tested. The three cases, although assumed previously as simple shear flows, turned out – owing to the rolls (Fig. 11) – to be more complex than simple shear flow, especially case b. That means that there are extensional flow components. According to the rheological experiments described earlier, the following equation for the yield stress could be chosen:

$$\tau_0 = \tau_0(w, \sigma, c_F) \ . \tag{9}$$

The shear stress $\tau_0(s,\sigma,c_F)$ determined with the experimental device can be converted into $\tau_0(w, \sigma, c_F)$ according to Eqs. (2) and (4), where the displacement, s, is replaced by the corresponding volume-specific energy input, w. This is only one possibility to model the flow behaviour of materials with a yield stress depending on the material's history of deformation.

The increase of the fraction of the immobilised liquid phase (ϕ_{im}) implicates a reduced rheologically effective moisture and, therefore, an increased pressure onto the solid matrix. According to the model of Raschka [35] the higher solid pressure causes an increase in the shear stress owing to Coulomb friction for the solid phase. Shear experiments performed by Felder [17] with watery pastes of limestone and Pural show that the shear stress mainly depends on the shear displacement and not on the speed of the measuring ring (tested for 0.05–30 mms^{-1}). Moreover, Felder [17] found that above a critical degree of moisture, peptisation of Pural pastes could not be observed, at least for the shear displacements considered in this study. For a given amount of solid there is only a limited surface to bind water, in spite of agglomeration and the increase in the number of fine particles by crushing the agglomerates. Water retained in the interior of the agglomerates must be considered as bound water from a rheological point of view. Above the critical degree of moisture there is probably too much free water left in the paste, so hardening cannot set in even though water is bound owing to the energy input.

When the Pural was kneaded before the shear experiments, the kneaded probes showed identical shear stress at smaller shear displacements. These results suggest that the structural changes primarily depend on the energy input into the sample, but not on the kind of energy input. That would imply that the hardening of Pural is not only induced by viscometric flow, but could also be caused by other types of flow. Flow-induced modifications make it hard (in comparison with so-called simple fluids) to realise a homogeneous consistency of the paste at the beginning of the experiment and, thus defined initial conditions, and to realise and

guarantee defined states of flow, stress and consistency (e.g.. degree of moisture, composition of the mixture) for the complete experiment. The evolution of the rolls (Fig. 11) indicates that there is not necessarily a plane shear flow in the shearing device as usually assumed for the analyses of rheometric measurements. Therefore, it is advisable to perform experiments with on-line registration of the structure and the flow pattern within the flowing paste to ensure the assumed experimental conditions [18, 19, 36–38]. The clear dependency of flow behaviour and deformation history is probably the reason for many cases of poor reproducibility of rheological experiments with pastes [17, 35].

In order to exclude that the observed rolls are not related to the onset of Taylor vortices, the Taylor criterion established for Newtonian fluids was checked. If Eq. (10) for the relevant critical number holds Taylor vortices do not appear:

$$\rho\omega r^{0.5}e^{1.5}/\eta < 41.3 \ , \qquad (10)$$

where ρ is the mass density, ω is the angular velocity, r is a characteristic length, e is the thickness of the sheared layer and η is the apparent viscosity. Owing to the high apparent viscosity (about 10^4–10^5 Pas) Eq. (10) is fulfilled and the observed vortices are, therefore, not caused by inertia effects.

The preparation treatment (before the shear experiments) might be responsible for the high standard deviations. Different temporal developments of the shear stress, especially at small shear displacements ($s < 1$ m) together with small energy inputs, are, therefore, probably caused by the originally (at $s = 0$ m) heterogeneous consistency of the paste. After sufficient deformation all the pastes should reach a homogeneous state [39, 40]. If the behaviour of the probe is modelled as a Bingham fluid, the dependency of the yield stress upon the volume -specific work, the normal stress and the average degree of moisture can be determined with the shear device of Felder [17]. This information can be used for rheological characterisation and for the design of apparatus and processes to handle these material systems. In order to achieve reliable process conditions (extrusion, pumping, etc.) it should be guaranteed that further energy input due to flow processes will not alter the consistency of the material and that all time-dependent effects are finished. Otherwise the prediction of the processes is problematic.

In future studies it should be tested whether the flow-induced aggregation processes can be described with theories of orthokinetic coagulation [28]. Orthokinetic coagulation means that the coagulation process rate is proportional to the collision frequency and this is again proportional to the shear rate. The coagulation process is accelerated by gentle stirring, which increases the collision frequency. At high shear rates larger moving units may form. At high rates of shear, the larger flocs become deformed and elongated (probably this is the formation of rolls). The larger moving units tend to sweep up other small particles in their path and hence, at moderate shear rates, if applied for sufficient time periods produce a steady-state aggregate size distribution. The existing data, two shear displacements in Fig. 10, are not sufficient to test the theories.

Conclusion

The results support the hypothesis that the structural changes (hardening, increase of the mean porosity) within the material during the peptisation mainly depend on the amount and not on the manner of the energy input. With the help of NMR spectra it was possible to differentiate two water phases. The fraction of the immobilised water increases with the shear displacement. Furthermore, crushing of aggregates of primary particles could be observed with particle size analysis. Both the crushing of solid particles and, hence, the increasing specific surface related to the solid mass and the formation of a three-dimensional structure, for example, a gel phase, are imaginable microscopic effects to bind water. On the macroscopic scale these processes cause hardening by peptisation and the high energy input due to the shear flow guarantees optimal dispersing and crushing, which could additionally intensify the peptisation. With MRI, flow-induced agglomerates that form during the shear experiment were detected. These and the formation of isolated rolls of material in the shear cell are responsible for the increase in the porosity. The structural changes (peptisation, agglomeration, increase in the fraction of fine particles, inhomogeneous consistency of the paste) make it difficult, when modelling the behaviour of a flowing paste, to determine experimentally the corresponding material constants or functions.

Usually shearing, especially with high normal stresses, guarantees intensive dispersion of the samples treated and leads to a homogeneous structure. It was, therefore, surprising that a process like the shear experiments described could turn a homogeneous unsheared sample (Fig. 10a) owing to the previously mentioned microscopic effects into a sample with large agglomerate as shown in Fig. 10b, provided sufficient energy input.

Generally a lot of assumptions and corrections for evaluation of rheometric measurements are made in order to obtain the real flow function of a material. It is problematic that the basic presuppositions can hardly be checked without the knowledge of the flow pattern in the rheometric device. That is why rheology combined with MRI offers such great possibilities.

The flow pattern realised in the shear device developed by Felder [17] might primarily appear to be a poorly controlled shearing deformation. This impression can be qualified or even invalidated with the results. Firstly, the analysis of Couette [37] and capillary [36] experiments has shown that they are not suitable for all pastes or concentrated suspensions because of demixing/internal flow, tearing apart and the flow patterns deviate from the assumed ones. That means the appearance of the isolated rolls is principally a problem of pastes and not of the shear device used. Secondly, Felder's shear device allows shear experiments to be performed with controlled normal stress and constant mean moisture of the sample, as the measuring volume can be sealed by an adjustable O-ring that ensures a hermetically sealed volume without any disturbing effects on the measurements of the normal and shear stress. These features are hard to realise with other rheometric devices. Therefore, a combination of Felder's shear device with MRI would be desirable.

Acknowledgements We thank the DFG, Bonn, (BU485/16), and the Fond der Chemischen Industrie, Frankfurt, for financial support and D. Müller, Bruker Analytische Meßtechnik GmbH, Rheinstetten, Germany, for his advice and technical support.

References

1. Barnes HA, Hutton JF, Walters K (1989) An introduction to rheology. Elsevier, Amsterdam
2. Pahl M, Gleissle W, Laun, H-M (1995) Praktische Rheologie der Kunststoff und Elastomere. VDI, Dusseldorf
3. Weipert D, Tscheuschner H-D, Windhab E (1993) Rheologie der Lebensmittel. Behrs, Hamburg
4. Ungarish M (1993) Hydrodynamics of suspensions. Springer, Berlin Heidelberg New York
5. Joseph DD, Renardy YY (1992) Fundamentals of two-fluid dynamics, part I: mathematical theory and applications. Springer, Berlin Heidelberg New York
6. Joseph DD, Renardy YY (1992) Fundamentals of two-fluid dynamics, part II: lubricated transport, drops and miscible liquids. Springer, Berlin Heidelberg New York
7. Bird RB (1987) Dynamics of polymeric liquids, part 1. Fluid mechanics. Wiley, New York
8. Bird RB, Dai GC, Yarusso BJ (1983) Rev Chem Eng 1:1
9. Barnes HA (1995) J Non-Newtonian Fluid Mech 56:221–251
10. Barnes HA (1995) J Non-Newtonian Fluid Mech 70:1–33
11. Gmachowski L (1996) J Colloid Interface Sci 178:80–86
12. Graham AL, Byron Bird R (1984) Ind Eng Chem Fundam 23:406–410
13. Graham AL, Steele RD, Byron Bird R (1984) Ind Eng Chem Fundam 23: 420–425
14. Schluentz EJ, Steffe JF, Ng PKW (2000) J Texture Stud 31:1
15. Briggs JL, Steffe JL (1997) J Texture Stud 28:5
16. Dolan KD, Steffe JL (1990) J Texture Stud 21:3
17. Felder R (1990) Dissertation, Universität Karlsruhe
18. Götz J (1994) Dissertation. Universität Karlsruhe
19. Götz J, Buggisch H, Peciar M (1993) J Non-Newtonian Fluid Mech 49: 251–275
20. Bloch F, Hansen WW, Packard M (1946) Phys Rev 70:476
21. Bloch F, Hansen WW, Packard M (1946) Phys Rev 69:127
22. Purcell M, Torrey HC, Pound RV(1946) Phys Rev 69:37
23. Callaghan PT (1991) Principles of nuclear magnetic resonance microscopy. Clarendon, Oxford
24. Abragam A (1961) Principles of nuclear magnetism. Clarendon, Oxford
25. Hills B, Takacs S, Belton P (1990) Food Chem 37:95–111
26. Zimmerman JR, Brittin WE (1957) J Phys Chem 61:1328–1333
27. Blümich B (2000) NMR imaging of materials. Clarendon, Oxford
28. Lagaly G, Schulz O, Zimehl R (1997) Dispersionen und Emulsionen. Steinkopff, Darmstadt
29. Garrecht H, Götz J (2001) Eur Patent EP 97937447.7
30. Bingham EC (1922) Fluidity and plasticity. McGraw-Hill, New York
31. Hill R (1959) The mathematical theory of plasticity. Clarendon Press, Oxford
32. Schmidt R (1932) Ing-Archiv 3:215
33. Schluentz EJ, Steffe J, Ng PKW (2000) J Texture Stud 31:41–54
34. Campo DT, Steffe J, Ng PKW (1997) Cereal Chem 74:489–494
35. Raschka K (1990) Dissertation. Universität Karlsruhe
36. Götz J, Kreibich W, Peciar M (2002) Rheol Acta, to be published
37. Götz J, Kreibich W, Peciar M, Buggisch H (2001) J Non-Newtonian Fluid Mech 98:117–139
38. Callaghan PT (1999) Rep Prog Phys 62:599–670
39. Buggisch H, Huth S (1997) Schriften Forschungsver Bau- Baustoffmaschinen 11:1–143
40. Huth S, Buggisch H (1998) 1st European Symposium on Process Technology in Pharmaceutical and Nutritional Sciences, PARTEC 98, Nuremberg, 10–12 March, pp 63–72